RESEARCH ARTICLE

Aggregation of high-frequency RBD mutations of SARS-CoV-2 with three VOCs did not cause significant antigenic drift

Tao Li[1] | Zhimin Cui[1,2] | Yunfei Jia[3,4] | Ziteng Liang[1] | Jianhui Nie[1] | Li Zhang[1] | Meng Wang[1] | Qianqian Li,[1] | Jiajing Wu[1] | Nan Xu[1] | Shuo Liu[1] | Xueli Li[1] | Yimeng An[1] | Pu Han[3] | Mengyi Zhang[1] | Yuhua Li[5] | Xiaowang Qu[6] | Qihui Wang[3,7] | Weijin Huang[1] | Youchun Wang[1]

[1]Division of HIV/AIDS and Sex-Transmitted Virus Vaccines, Institute for Biological Product Control, National Institutes for Food and Drug Control (NIFDC), Beijing, China

[2]Key Laboratory of Research on Quality and Standardization of Biotech Products, National Health Commission, Beijing, China

[3]CAS Key Laboratory of Pathogen Microbiology and Immunology, Institute of Microbiology, Chinese Academy of Sciences, Beijing, China

[4]Department of Veterinary, College of Veterinary Medicine, Shanxi Agricultural University, Jinzhong, China

[5]Department of Arboviral Vaccine, Institute for Biological Product Control, National Institutes for Food and Drug Control (NIFDC), Beijing, China

[6]Laboratory of Virology and Immunology, Translational Medicine Institute, the First People's Hospital of Chenzhou, University of South China, Chenzhou, China

[7]Savaid Medical School, University of Chinese Academy of Sciences, Beijing, China

Correspondence
Yuhua Li, Department of Arboviral Vaccine, Institute for Biological Product Control, National Institutes for Food and Drug Control (NIFDC), No. 31 Huatuo St, Daxing District, Beijing 102629, China.
Email: liyuhua@nifdc.org.cn

Xiaowang Qu, Laboratory of Virology and Immunology, Translational Medicine Institute, the First People's Hospital of Chenzhou, University of South China, Chenzhou 423000, China.
Email: quxiaowang@163.com

Qihui Wang, CAS Key Laboratory of Pathogen Microbiology and Immunology, Institute of Microbiology, Chinese Academy of Sciences, Beijing 100101, China.
Email: wangqihui@im.ac.cn

Weijin Huang and Youchun Wang, Division of HIV/AIDS and Sex-Transmitted Virus Vaccines, Institute for Biological Product Control, National

Abstract

Variants of SARS-CoV-2 continue to emerge, posing great challenges in outbreak prevention and control. It is important to understand in advance the impact of possible variants of concern (VOCs) on infectivity and antigenicity. Here, we constructed one or more of the 15 high-frequency naturally occurring amino acid changes in the receptor-binding domain (RBD) of Alpha, Beta, and Gamma variants. A single mutant of A520S, V367F, and S494P in the above three VOCs enhanced infectivity in ACE2-overexpressing 293T cells of different species, LLC-MK2 and Vero cells. Aggregation of multiple RBD mutations significantly reduces the infectivity of the possible three VOCs. Regarding neutralization, it is noteworthy that E484K, N501Y, K417N, and N439K predispose to monoclonal antibodies (mAbs) protection failure in the 15 high-frequency mutations. Most importantly, almost all possible VOCs (single RBD mutation or aggregation of multiple mutations) showed no more than a fourfold

Institutes for Food and Drug Control (NIFDC), No. 31 Huatuo St, Daxing District, 102629 Beijing 102629, China.
Email: huangweijin@nifdc.org.cn and wangyc@nifdc.org.cn

decrease in neutralizing activity with convalescent sera, vaccine sera, and immune sera of guinea pigs with different immunogens, and no significant antigenic drift was formed. In conclusion, our pseudovirus results could reduce the concern that the aggregation of multiple high-frequency mutations in the RBD of the spike protein of the three VOCs would lead to severe antigenic drift, and this would provide value for vaccine development strategies.

KEYWORDS
cell–cell fusion, convalescent serum, infectivity, neutralization, pseudotyped virus, SARS-CoV-2

1 | INTRODUCTION

Concerns about severe acute respiratory syndrome coronavirus 2 (SARS-CoV-2), the root of the current coronavirus pandemic, have been ongoing. As of November 30, 2021, the global coronavirus disease 2019 (COVID-19) pandemic had resulted in more than 259 million confirmed cases and more than 5.18 million deaths (https://covid19.who.int/). SARS-CoV-2 is an RNA virus with a high mutation rate despite its own replication error correction capability. Over the past year, more than 28 000 mutations and 5000 insertion/deletion changes were detected for this virus (https://bigd.big.ac.cn/ncov/variation/annotation). Spike protein is critical for SARS-CoV-2 to attach to and infect target cells. The receptor-binding domain (RBD) within the spike protein is the most important region and is mainly responsible for binding to the ACE2 receptor in target cells. It is also the primary target of monoclonal antibodies (mAbs) and one of the fastest evolving regions.[1,2] Therefore, mutations in this region can affect the infectivity and antigenicity of the virus,[3–5] which may lead to reduced vaccine efficacy and the emergence of reinfections.[6] As of March 2021, at the beginning of this study, the most widely spread single mutant variant was N501Y, accounting for more than 820 000 (46%) of the ~1.77 million SARS-CoV-2 sequences uploaded in the GISAID database (https://www.epicov.org). The amino acid change N501Y enhances the affinity of the RBD to ACE2[1,7–9] and is more transmissible than other mutant variants.[10,11] Another important amino acid mutant is E484K, reaching more than 5.7% of total sequences. This mutation causes a significant decrease in the effectiveness of neutralizing antibodies and vaccine protection.[12] As of March 2021, the 15 most commonly observed mutations in the RBD were as follows: V367F, P384L, K417N, N439K, L452R, Y453F, S477N, S477R, T478K, E484K, S494P, N501T, N501Y, A520S, and A522S, which were located at 13 sites in the RBD. All of these 15 mutations are mutant-prone and may readily occur in other variants.

Mutation statistics by the National Genomics Data Center (https://ngdc.cncb.ac.cn/) and other reports showed that the rate of viral mutation of the spike protein has continued to increase since the

SARS-CoV-2 pandemic[13] and new variants continue to emerge. Based on this, the World Health Organization (WHO) classifies variants into variants of concern (VOCs) and variants of interest (VOI) based on the degree of variability in transmissibility, virulence, or diagnostic/therapeutic/vaccine efficacy. Mutations such as N501Y, S477N, N439K, L452R, E484K, K417N, T478K, and K417T were observed in VOCs and VOIs, and these sites were listed as RBD high-frequency mutation sites, suggesting that these sites are mutation-prone. Three VOC, namely Alpha, Beta, and Gamma, were identified by the WHO at the beginning of this study. The Alpha variant, also known as B.1.1.7, 20I/501Y.V1, was first discovered in the UK in September 2020 and has since been detected in 137 countries and generated global attention. The Beta variant (B.1.351, GR/501Y.V2) became endemic after the first wave of the SARS-CoV-2 epidemic in South Africa in May 2020 and rapidly replaced other variants as the dominant variant, having spread across 97 countries worldwide. The other of the VOC, Gamma (P.1 or GH/501Y.V3), has become the most prevalent variant in Brazil, with a prevalence of 91% in January 2021, and detection in 55 countries including Japan (https://outbreak.info/situation-reports#voc). All three VOCs contain the N501Y mutation that makes the virus more infectious. Furthermore, the VOCs are constantly mutating and evolving. For example, the RBD of spike protein in the Alpha variant has since evolved a new mutation E484K, which has also appeared in the Beta and Gamma variants. Notably, variants from different regions have evolved identical mutations, often resulting from the combination of multiple RBD loci. This suggests that these mutation-prone sites in the RBD have an increased probability of forming new variants when combined with other variants during evolution. Some new variants may exhibit functional changes such as infectivity and antigenicity, which pose new challenges for pandemics.

To predict whether the function of possible mutants of the three VOCs would be changed, we constructed mutant pseudotyped viruses with single and multiple mutants of the top 15 high-frequency mutations in the RBD combined with three VOCs (Alpha, Beta, and Gamma), and analyzed the impact on infectivity and antigenicity.

2 | MATERIALS AND METHODS

2.1 | Plasmid construction

The expression plasmid harboring the SARS-CoV-2 spike gene (GenBank accession no: MN908947.3) was optimized using mammalian codons, and the DNA fragment was constructed on the eukaryotic expression vector pcDNA3.1 using *Bam*HI and *Xho*I digestion sites to obtain the plasmid pcDNA3.1-SARS-CoV-2 spike. In total, 72 mutation plasmids were constructed on this basis. The site mutation method was the same as that used in our previous studies.[14,15] The specific mutation sites and corresponding primers (synthesized by China Biotechnology) are shown in Table S2.

A total of 14 plasmids expressing ACE2 protein were constructed, including human (BAB40370.1), mink (QNC68911.1), dog (MT663955), cat (MT663959), pangolin (XP_017505746.1), pig (NP_001116542.1), mouse (ABN80106.1), bat (KC881004.1) and bovine (NP_001116542.1) plasmids,[16] by China General Biological Corporation. All protein-coding sequences were optimized with mammalian codons and tagged with FLAG tags at the carboxyl terminus. The target sequences were inserted into the eukaryotic expression vector pcDNA3.1 at *Bam*HI, *Xho*I, or *Eco*RI digestion sites.

2.2 | Cells

The 293T (American Type Culture Collection [ATCC], CRL-3216), Huh-7 (Japanese Collection of Research Bioresources [JCRB], 0403), Vero (ATCC, CCL-81), LLC-MK2 (ATCC, CCL-7), and 293T-hACE2 cells were cultured using Dulbecco's modified Eagle's medium (DMEM, high sugar; Hyclone). DMEM was supplemented with 100 U/ml penicillin–streptomycin solution (GIBCO), 20 mM n-2 hydroxyethylpiperazinen-2-ethanesulfonic acid (HEPES, GIBCO), and 10% FBS (Pansera ES, PAN-Biotech). Cells were cultured at 37°C in a 5% CO_2 environment with trypsin-EDTA (0.25%, GIBCO) and isolated for passaging every 2–3 days. Cells from different species overexpressing ACE2 were prepared as follows: transiently expressed cell lines were obtained by transiently transfecting 293T cells with 10 μg ACE2 plasmid using Lipofectamine 3000 transfection reagent (Invitrogen) in T25 flasks, for example. The transient ACE2-expressing cell lines were used for subsequent experiments after incubation at 37°C for 24 h in a 5% CO_2 incubator.

2.3 | Preparation of pseudotyped viruses

SARS-CoV-2 pseudotyped viruses and site mutant pseudotyped viruses were constructed in accordance with the method described in our previous study.[15] The day before transfection, 293T cells were digested and their concentration was adjusted to $5–7 \times 10^5$ cells/ml.[14,15] Then, 15 ml of the cell culture medium was transferred to T75 cell culture flasks and incubated overnight in an incubator at 37°C and 5% CO_2. When cells reached 70%–90% confluence, the medium was discarded and 15 ml of

G *ΔG-vesicular stomatitis virus (VSV G pseudotyped virus, Kerafast) at a concentration of 7.0×10^4 $TCID_{50}$/ml was used for infection. The cells were simultaneously transfected with 30 μg of the SARS-CoV-2 S protein expression plasmid, following the instructions provided with the Lipofectamine 3000 transfection reagent (Invitrogen), and then incubated at 37°C with 5% CO_2. After 4–6 h, the cell culture medium was discarded and the cells were gently washed twice with phosphate-buffered saline (PBS) + 2% fetal bovine sera (FBS). Next, 15 ml of fresh complete DMEM was added to T75 cell culture flasks, which were incubated at 37°C and 5% CO_2. After 24 h, culture supernatants containing SARS-CoV-2 pseudovirus were harvested, filtered, divided, and frozen at −80°C for use in subsequent experiments.

2.4 | Quantification of pseudotyped viral particles by reverse-transcription polymerase chain reaction (RT-PCR)

Before quantification using RT-PCR, all pseudotyped viruses were purified by 25% sucrose buffer and centrifuged at 100 000*g* for 3.5 h.[14] Viral RNA was extracted from 140 ml of purified pseudotyped viruses using the QIAamp Viral RNA Mini Kit (QIAGEN, Cat#52906). Viral RNA was extracted using the SuperScript III First-Strand Synthesis System and the RT-PCR kit (Invitrogen, Cat#18080-051) was used for reverse transcription. The virus was quantified by real-time PCR using TB Green Premix ExTaqII (TaKaRa, Cat#RR820A) in accordance with the supplier's instructions. The P protein gene of VSV was cloned into the vector pCDNA3.1(+) as a standard to calculate the corresponding viral copy number.

2.5 | Pseudotype virus infection experiment

RNA from the SARS-CoV-2 pseudovirus and site mutant pseudovirus was extracted using the QIAamp Viral RNA Mini kit as described above and then reverse-transcribed to obtain complementary DNA (cDNA). After quantification by real-time quantitative fluorescence PCR, the pseudovirus was diluted to the same particle number and added to 96-well cell culture plates at 100 μl per well. After digestion of the 293T cell line and ACE2-overexpressing cells with trypsin, 2×10^5/ml cells were added to each well. Chemiluminescence assays were then performed after incubation for 24 h at 37°C in a 5% CO_2 incubator. Detailed procedures are described in our previous publication.[15] Briefly, 100 μl of luciferase substrate (Perkin-Elmer) was added to the wells, incubated and shaken for 2 min at room temperature, and then transferred to a test white plate for detection using a luminometer (Perkin-Elmer). Each set of experiments was repeated three times.

2.6 | mAbs

A total of 12 mAbs that neutralize the SARS-CoV-2 S protein were used. Among them, mAb CB6 was provided by Jinghua Yan of the Institute of

Microbiology, Chinese Academy of Sciences; mAbs DXP-593 and DXP-604 were provided by Sunney Xie of Peking University; mAbs 03-10D12-1C3, 03-9A8, 05-9G11, 09-4E5-1G2, and 09-7B8 were provided by Beijing Biocytogen Co., Ltd. following immunization of mice with spike protein followed by hybridoma cell fusion screening; mAb 9MW3311-MW07-LALA was provided by Beijing Kohnoor Science & Technology Co., Ltd.; mAbs AM128 and AM180 were provided by ACROBiosystems Co., Ltd.; mAb AbG3 was provided by Fipen Biologics Co., Ltd.

2.7 | Sera of convalescent patients

Twenty sera, collected between March and October 2020, from convalescent patients cured of 2019-nCoV infection, were provided by Xiaowang Qu at the University of South China. All volunteers signed an informed consent form. Ethics approval was obtained for this study by the Translational Medicine Institute, University of South China (V1.0, 203301).

2.8 | Vaccine volunteer sera

Five cases of recombinant SARS-CoV-2 vaccine (Ad5-nCoV-Spike) inoculated serum provided by Canxino Co., Ltd., which has been conditionally marketed in China; four cases of SARS-CoV-2 mRNA vaccine (LPP/mRNA-Spike) inoculated serum provided by Stemirna Therapeutics Co., Ltd., which has completed clinical phase I. Written informed consent was obtained from each individual for the collection of serum.

2.9 | Guinea pig immune sera

The strategy for vaccination of guinea pigs included one dose of DNA plasmid and two doses of a SARS-CoV-2 pseudotyped virus. Female guinea pigs of 250 g were immunized with 200 μg of spike-DNA plasmid and treated with intramuscular electrotransfer. After 2 weeks, they were immunized with pseudotyped spike-VSV (the virus was ultrapurified and the nucleic acid quantified by the same method as described for the previous RT-PCR). The pseudotyped virus particles, comprising 2 μg of viral nucleic acid mixed in equal proportions with aluminum adjuvant, were injected subcutaneously into guinea pigs. After another 2 weeks, the animals were immunized with a third injection of the pseudotyped virus at the same dose as before, and the immune sera were extracted from the guinea pigs 2 weeks later. The protocol for this animal study was approved by the Ethical Review Committee for Animal Welfare of The National Institutes for Food and Drug Control.

2.10 | Pseudotype virus neutralization test

The test antibody or serum samples are first diluted with PBS solution, then the samples were diluted in a total of six consecutive gradients using fresh DMEM containing serum in threefold gradients, followed by coincubation with VSV pseudotyped virus solution. Virus control wells and cell control wells were included on each 96-well plate. The virus solution (not the test sample) was added to the virus control wells, while only the complete medium (not the virus solution) was added to the cell control wells. After the addition of samples, the 96-well plates were incubated at 37°C for 1 h, and then dispersed Huh7 cells (2×10^4 cells/100 μl) were added to each well. Chemiluminescence was detected after incubation at 37°C and 5% CO_2 for 24 h. The effect of mAbs and sera on the inhibition of pseudotyped virus entry was evaluated by detecting a decrease in luciferase expression.[15] The EC_{50} or NT_{50} values for samples were calculated using the Reed–Muench method.

2.11 | Quantitative detection of SARS-CoV-2 spike protein

Packed pseudotyped viruses were collected and viral RNA was first extracted as previously described, reverse-transcribed into cDNA, then viral nucleic acid quantification was performed by real-time fluorescence PCR. Pseudotyped viruses with the same viral particle number were used for subsequent quantification of the spike protein. Using the sandwich enzyme-linked immunosorbent assay method, standards and samples to be tested were added in accordance with the instructions of the Acro BIOSYSTEMS kit (Cat#TAS-K020), and biotin-labeled anti-SARS-CoV-2 spike protein antibody (Cat#RAS020-C03) was added at the end of the incubation to form antibody–antigen–antibody complexes. After washing the plate, streptavidin-horseradish peroxidase (HRP) was added and the chromogenic solution was added at the end of the incubation. The HRP catalyzed the substrate to produce a blue substance, and the solution turned yellow when the termination solution was added. The absorbance value (OD) was then measured at 450 nm. OD values were positively correlated with the SARS-CoV-2 spike protein content.

2.12 | Cell–cell fusion assay

Two types of cells were used for fusion experiments, and 293T cells were first transfected with spike protein sequences carrying the D614G variant or a combined single mutant and the GFP1–7 RLN plasmid. Cells stably expressing human ACE2 were transfected with the GFP8–11 RLC plasmid as recipient cells. Cells were cultured at 37°C and 5% CO_2 for 24 h and then isolated with trypsin. Donor and recipient cells were mixed in a 1:1 ratio and seeded in 96-well plates. Fluorescence values reflecting GFP expression were monitored 3 h after mixing. The GFP signal was detected using a BioTek Cytation 5V instrument, as described previously.[17,18]

2.13 | Gene cloning, expression, and protein purification

The pCAGGS plasmid expressing human ACE2-mFc (residues 1–740, GenBank: NP_001358344) protein for surface plasmon resonance

(SPR) was constructed in our recent work.[19] The plasmid was transiently transfected into HEK293T cells (ATCC CRL-3216) using PEI and then, 72 h later, the cell supernatants were collected, concentrated, and used in the SPR assays.

The DNA sequence encoding hACE2 (residues 19–615, GenBank:NP_001358344) was inserted into the Baculovirus transfection vector pFastBac1 (Invitrogen) using the EcoRI and XhoI restriction sites. The gp67 signal peptide sequence was added to the N-terminus of the hACE2 gene for protein secretion, and the Hexa-His tag sequence was added to the C-terminus of the hACE2 sequence for protein purification. The hACE2 protein was expressed using the Bac-to-Bac Baculovirus expression system and used for crystallization. The pFastBac1-hACE2 plasmids were transformed into DH10Bac E. coli to produce recombinant bacmids. Transfection of the bacmids using FuGENE 6 Transfection Reagent (Promega) and virus amplification was carried out in Sf9 cells, and the proteins were expressed in High Five cells. The supernatants were collected 48 h postinfection.[20]

The DNA sequences encoding SARS-CoV-2 WT RBD (spike residues 319–541, GISAID: EPI_ISL_402119) were inserted into the pCAGGS vector with IL10 signal peptide sequence at the N-terminus and the Hexa-His tag at the C-terminus. The SARS-CoV-2 variant RBD plasmids (including Alpha RBD, Beta RBD, Gamma RBD, Alpha A520S RBD, Beta A520S RBD, and Gamma A520S RBD) were completed by subcloning. The supernatants containing hACE2 or RBD proteins were purified via affinity chromatography using a HisTrap HP 5 ml column (GE Healthcare) and the target proteins were eluted in an elution buffer composed of 20 mM Tris (pH 8.0), 150 mM NaCl, and 300 mM imidazole. The samples were then purified using gelfiltration chromatography on a HiLoad 16/600 Superdex 200PG column (GE Healthcare) in a buffer containing 20 mM Tris (pH 8.0) and 150 mM NaCl.[21]

2.14 | Crystallization

The sitting-drop method was used to obtain high-resolution Gamma-A520S RBD/hACE2 complex crystals. In detail, the purified complex proteins were concentrated to 10 mg/ml. Then, 0.8 ml protein was mixed with 0.8 ml reservoir solution. The resulting solution was sealed and equilibrated against 100 ml of the reservoir solution at 18°C. High-resolution Gamma-A520S RBD/hACE2 complex crystals were grown in 0.1 M MES (pH 6.0), 15% w/v PEG 4000.

2.15 | Data collection and structure determination

Reservoir solution supplemented with 20% (v/v) glycerol was prepared as an antifreezing buffer for freezing crystals. Crystals were picked up from the groove by using a mini loop and soaked in the antifreezing buffer for a few seconds. Then, crystals were picked up and frozen by soaking in liquid nitrogen. Diffraction data were collected at the Shanghai Synchrotron Radiation Facility (SSRF) 02U1. The data set was processed with HKL2000 software as previously

described.[22] The structure of the Gamma-A520S RBD/hACE2 complex was determined by the molecular replacement method using Phaser [23] with a previously reported complex structure of the SARS-CoV-2-RBD complex with human ACE2 (PDB: 6LZG). The atomic models were completed using Coot[24] and refined with Phenix refine in Phenix,[22] and the stereochemical qualities of the final models were assessed using MolProbity. All structural figures were generated using Pymol software (https://pymol.org/2/).

2.16 | SPR analysis

The SPR assays were performed to test the interactions between mFc-fused human ACE2 and SARS-CoV-2 variant RBDs using a BIAcore 8 K (GE Healthcare) with a CM5 chip (GE Healthcare) at 25°C in single-cycle mode. SARS-CoV-2 WT RBD was used as a positive control. All proteins used for kinetic analysis were exchanged to the PBST buffer (10 mM Na_2HPO_4, 2 mM KH_2PO_4, pH 7.4, 137 mM NaCl, 2.7 mM KCl, 0.005% Tween 20) and the anti-mIgG antibody (Cytiva) was preimmobilized on the CM5 chip using standard amine coupling chemistry with a 50 μg/ml concentration. Concentrated supernatant containing hACE2-mFc protein was captured on the chip using this immobilized antibody. Various concentrations of RBDs (6.25, 12.5, 25, 50, 100 nM) then flowed through the chip and the real-time response was recorded to evaluate hACE2 binding. The chip was regenerated after each reaction using glycine (pH 1.7). The equilibrium dissociation constants (binding affinity, K_D) for each pair of interactions were calculated using BIAcore 8K® evaluation software (GE Healthcare). The K_D values were calculated using the model of 1:1 (Langmuir) binding mode. These results were then visualized using Origin 2021.

2.17 | Statistical analysis

GraphPad Prism 8.0 (GraphPad Software) was used for plotting and statistical analysis. One-way ANOVA test and Holm–Sidak's multiple comparison test were used to analyze between-group differences. p values less than 0.05 were considered to be significant. The data are presented as the mean ± standard error for the sample mean (SEM) of at least three independent experiments. *$p < 0.05$, **$p < 0.01$, ***$p < 0.005$, ****$p < 0.001$, ns indicates no significant difference.

3 | RESULTS

3.1 | Construction of possible variants based on Alpha, Beta, and Gamma variants

With the continued spread of the COVID-19 epidemic, the Alpha, Beta, and Gamma variants have become the endemic VOCs (Figure 1A, data from GISAID), containing 9, 8, and 12 mutations on the S protein, respectively (as shown in Figure 1B). We screened the
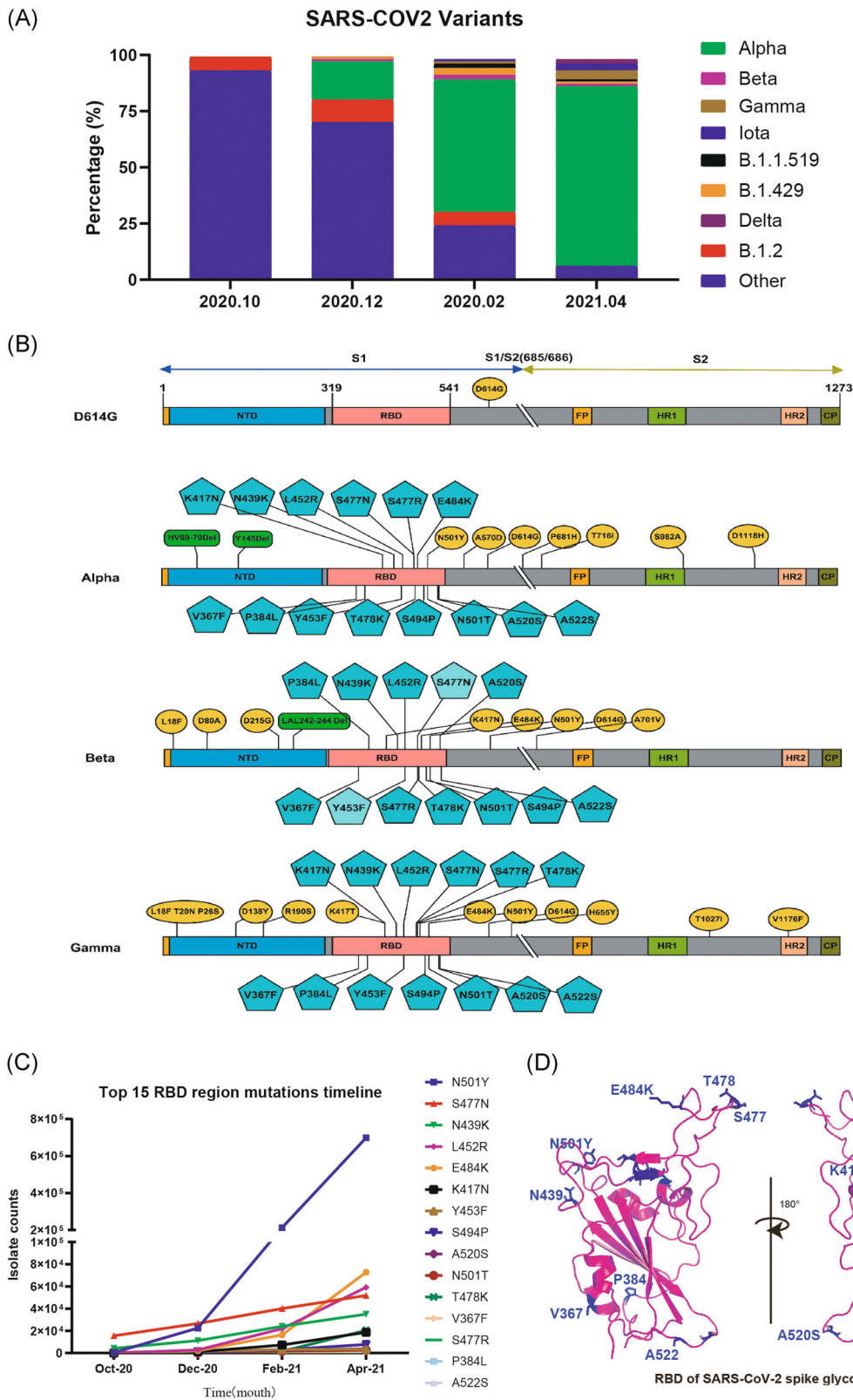
FIGURE 1 Schematic diagram of the changes in epidemic variants and the RBD mutation site and amino acid changes in this study. (A) Changes in the proportion of major variants of SARS-CoV-2 over time. (B) Schematic diagram of the 15 mutations with the highest mutation frequencies in the RBD over time. (C) Schematic diagram of mutations in the D614G, Alpha, Beta, and Gamma variants, where the pentagon represents the amino acid mutations introduced on the pseudotyped virus spike protein in this study. (E) The RBD of SARS-CoV-2 spike glycoprotein was colored in magenta. The 15 most commonly observed mutations in the RBD were as follows: N501Y, S477N, N439K, L452R, E484K, K417N, Y453F, S494P, A520S, N501T, T478K, V367F, S477R, P384L, and A522S, which were located at 13 sites in the RBD. Gray was used to indicate the positions of amino acids (V367, P384, T478, L452, S494, A520S, and A522) in the RBD structure. RBD, receptor-binding domain

top 15 high-frequency mutations located at 13 sites of the RBD (Figure 1C), as determined from the GISAID database as of March 2021. Pseudotyped viruses were constructed with single amino acid mutations (Figure 1B), reflecting the top 15 mutations in the RBD combined with the three VOCs (Alpha, Beta, and Gamma) (Figure 1D). Pseudotyped viruses were also constructed by aggregating the amino acid mutations in the order of the first 13 high-frequency mutations in the three VOCs followed by N501Y, S477N, N439K, L452R, E484K, K417N, Y453F, S494P, A520S, T478K, V367F, P384L and A522S (Figure 1D). The D614G strain has replaced the SARS-CoV-2 (2019-nCoV) variant as a globally prevalent variant,[25–27] we used the D614G strain as the control reference in this study. All the pseudo-virus variant constructs used in this study are detailed in Table S1.

3.2 | The infectivity of possible variants of the three VOCs

First, we focused on exploring changes in the infectivity of possible variants in several primate cells (Huh-7, LLC-MK2, and Vero) susceptible to infection with SARS-CoV-2 and four 293T-hACE2/Furin/TMPRSS2/Cathepsin L stably transfected cell lines containing SARS-CoV-2 infection-associated enzymes.[28–31] Compared with the corresponding three VOCs, among the possible Alpha variants, Alpha +A520S showed a significant increase in infectivity of more than fourfold in LLC-MK2 and Vero cells. Alpha+S494P and Alpha+V367F also enhanced infectivity within fourfold (Figure 2A). Among the possible Beta variants, the Beta+V367F pseudovirus variant showed nearly fourfold enhanced infectivity, especially in Huh7 and LLC-MK2 cells, and Beta+S494P and Beta+A520S showed similar effects (Figure 2B). Among the possible Gamma variants, the Gamma+A520S variant showed the most significant increase in infectivity, approaching or even exceeding fourfold in all the cell lines (Figure 2C). Reassuringly, the infectivity of possible Alpha variants aggregated with the top five high-frequency mutations by order did not detectably increase. However, when the combined mutations reached 6th-Y453F and beyond (Figure 2A), the infectivity decreased, with infectivity rebounding slightly when combined with the V367F mutation. As the Beta and Gamma variants possess three mutations in the RBD region, they showed a decrease in infectivity when combined with the second mutation, which was particularly evident in hACE2-overexpressing 293T cells (Figure 2B,C). These findings suggested that the prevalence of variants with multiple high-frequency substitutions in the RBD is less likely to occur in nature. Besides, Alpha mutant pseudovirus variants were no significantly reduction infectious in 293T-hACE2+Furin stable-transformed cell lines (Figure 2A), a phenomenon also observed in possible Beta variants aggregated with multiple substitutions (Figure 2B). This suggested that Alpha and Beta mutant pseudovirus variants pose a risk of infection in cells with high ACE2 and Furin enzyme expression.

SARS-CoV-2 not only is transmissible between humans but also shows some infectious ability in animals such as minks,[32] bats, and pangolins were probably wildlife hosts of SARS-CoV-2.[33,34] We thereby investigated whether combinations of mutated possible variants cause changes in infectivity in different species to determine the risk of new zoonotic infections and expanded transmission. We transiently expressed ACE2 receptors of 14 different species in 293T cells to investigate the effects of Alpha, Beta, and Gamma possible variants on the infectivity of ACE2 cells of different species. Similar to the infectivity results for susceptible mammalian cell lines, the Alpha, Beta, and Gamma possible variants were significantly less infectious compared with the corresponding VOCs after combining multiple high-frequency mutations (Alpha possible variants superimposed to the 6th-Y453F mutation start to decline, Beta and Gamma possible variants superimposed to the 2nd-N439K mutation start to decline) (Figure 3). Notably, Alpha+A520S, Alpha+S494P, Beta+V367F, and Gamma+A520S possible variant pseudoviruses were significantly more infectious in 293T cells with high ACE2 receptor expression in most species (Figure 3), suggesting that these variants deserve special attention if they occur in nature. To further verify the effect of the three mutations, S494P, V367F, and A520S, on infectivity, we introduced a single-site mutation into the D614G pseudovirus variants individually and explored the changes in infectivity in the above cell lines. The results showed that the D614G + A520S possible variant had significantly enhanced infectivity in Calu-3 and Huh7 cells (Figure S1A). Furthermore, among the results from 293T-ACE2 cells of different species that were zoophilic, three mutant variants—S494P, V367F, and A520S—were particularly enhanced in infectivity in cells expressing mouse ACE2, reaching or approaching four-fold (Figure S1B), and these mutant variants deserve extra attention to prevent the emergence of new zoonotic transmissions.

3.3 | Effect of S494P, A520S, and V367F substitutions on spike protein expression on pseudotyped virus and cell–cell fusion

To further investigate the mechanism responsible for the change in infectivity of the S494P, A520S, and V367F mutations in the D614G, Alpha, Beta, and Gamma variants, we first examined the difference in the amount of spike protein under quantitative conditions for the pseudotyped virus. The results showed no significant difference in the amount of spike protein on the pseudotyped virus compared with the D614G strain and the three corresponding VOCs (Figure 4A). We could thereby exclude the possibility that the enhanced infectivity was due to an increased amount of spike protein formed on the viral surface.

The effect of pseudovirus variants on cell–cell fusion secondary to enhanced infectivity was further explored. The results showed that the S494P, A520S, and V367F mutant variants could enhance the intensity of intercellular fusion, with the A520S mutation, in particular, enhancing fusion more than twofold in the four mutant variant profiles of D614G, Alpha, Beta, and Gamma (Figure 4B). The same trend can be confirmed by cell–cell fusion of GFP expression (Figure S1C). These suggested that the increased infectivity of pseudovirus variants after the addition of S494P, A520S, and V367F
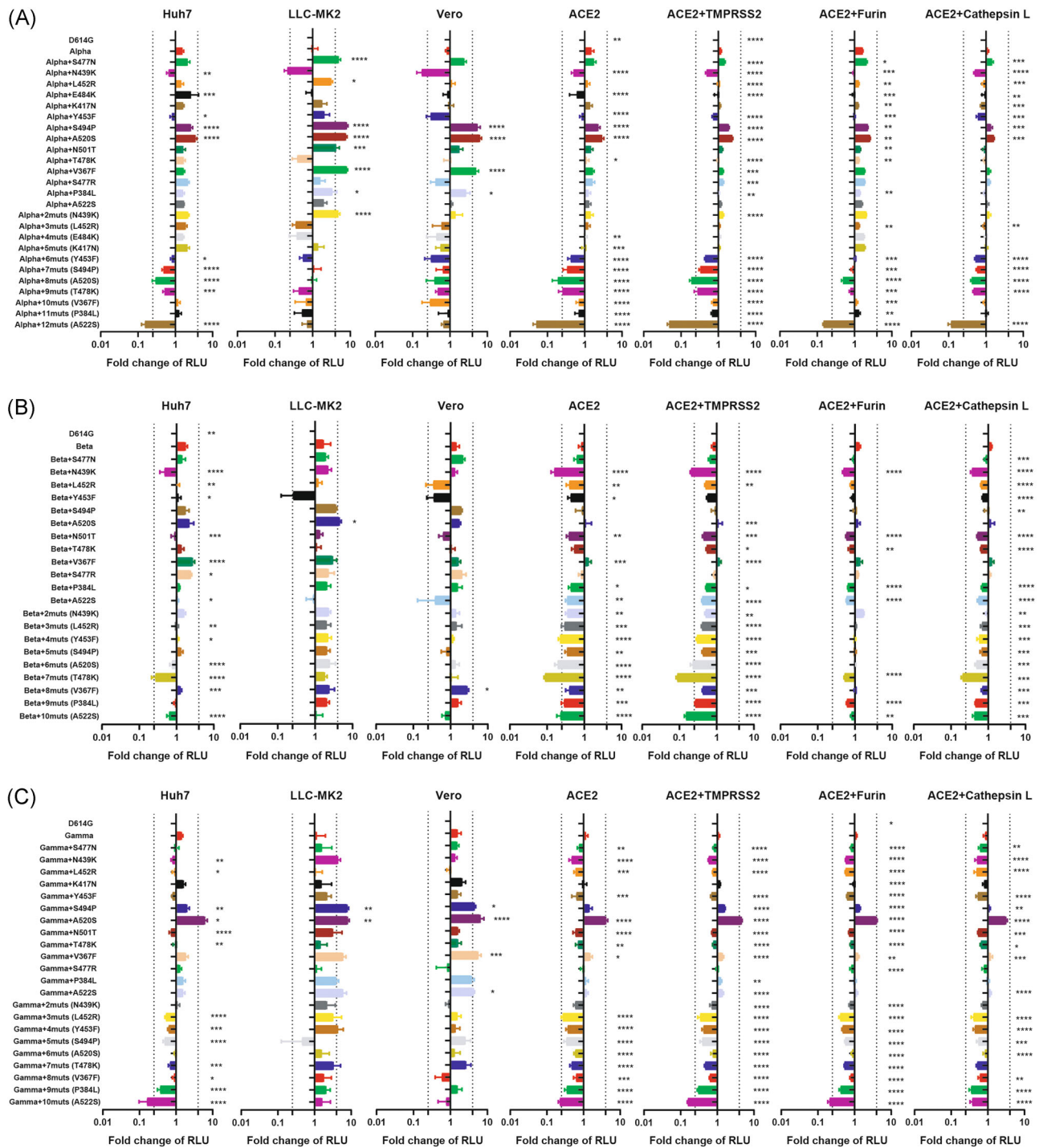
FIGURE 2 Infectivity changes of different possible pseudotyped variants in susceptible cell lines. Infectivity effects of Alpha (A), Beta (B), and Gamma (C) natural variants and their possible mutants were analyzed in susceptible Huh-7, LLC-MK2, and Vero cells and 293T cells transiently expressing ACE2, ACE2 + TMPRSS2, ACE2 + Furin, and ACE2 + Cathepsin L. The variants and their possible mutant strains were first diluted by nucleic acid quantification to the same number of viral particles before infecting the cells. The RLU values, determined for the infected cells by detecting the variants and their possible mutant strains, were compared with the reference strain D614G. A fourfold difference was considered significant; the dashed lines in the graph represent a 0.25 or fourfold change compared with strain D614G, respectively. As an example of nomenclature, Alpha+2muts (N439K) represents the first two mutations with the highest mutation frequency introduced on the Alpha variant and the last site added is N439K. p values were calculated using the respective variants of concern as the control. Unless otherwise stated, all experiments were performed in triplicate (mean ± SEM). *$p < 0.05$, **$p < 0.01$, ***$p < 0.005$, ****$p < 0.001$
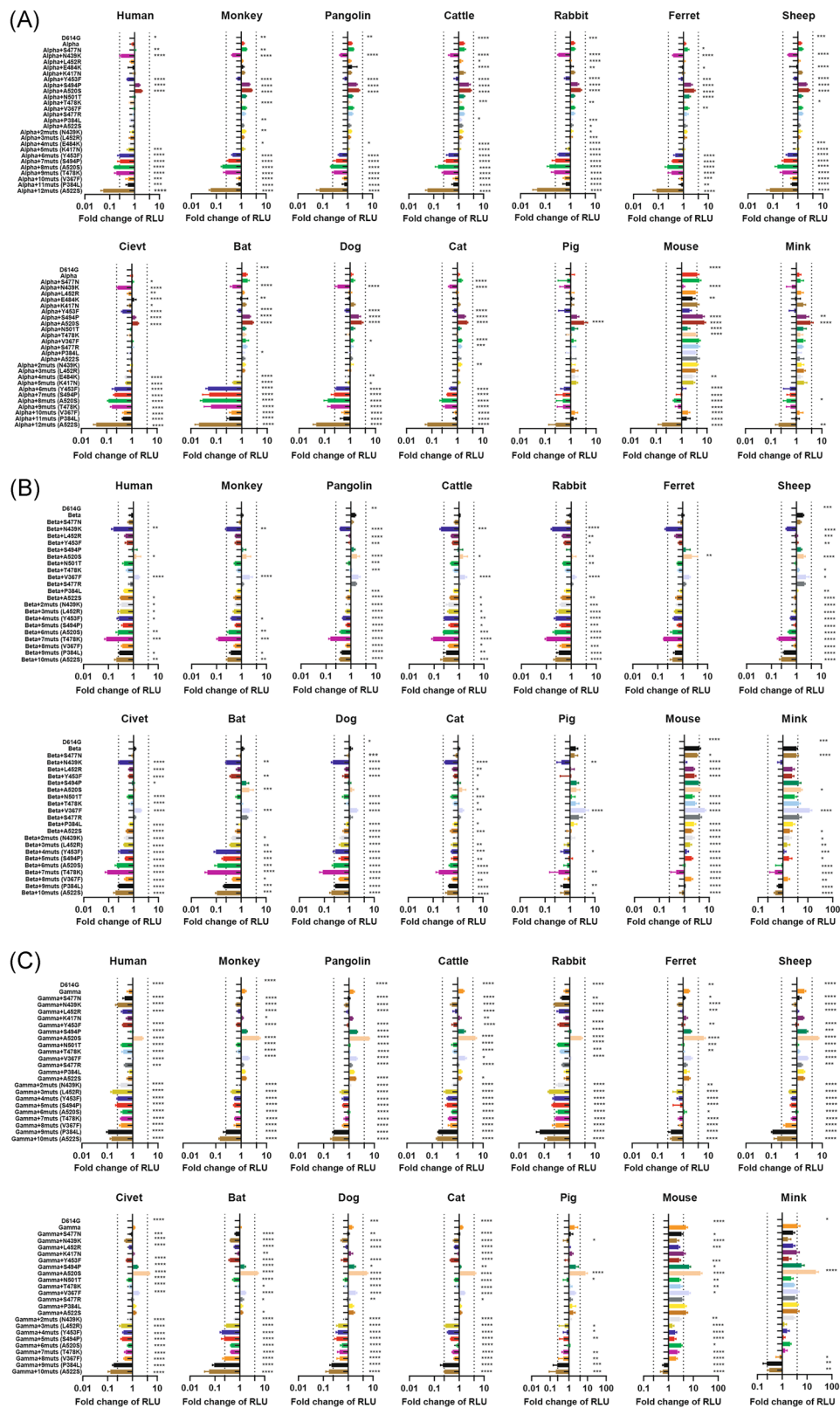
FIGURE 3 Infectivity changes of possible mutant pseudotyped viruses in ACE2-overexpressing cells of different species. The infectivity of Alpha (A), Beta (B), and Gamma (C) natural variants and their possible mutant strains was analyzed in 293T cells transiently expressing ACE2 from 14 species. The variants and mutant strains were first diluted to the same number of viral particles by nucleic acid quantification and then infected with cells, and the RLU values of the infected cells of the variants and their possible mutant strains were compared with the reference strain D614G by an infection assay. A fourfold difference was considered significant; the dashed lines in the graph represent a 0.25- or 4-fold change compared with strain D614G, respectively. p values were calculated using the respective variants of concern as the control. Unless otherwise stated, all experiments were performed in triplicate (mean ± SEM). $*p < 0.05$, $**p < 0.01$, $***p < 0.005$, $****p < 0.001$
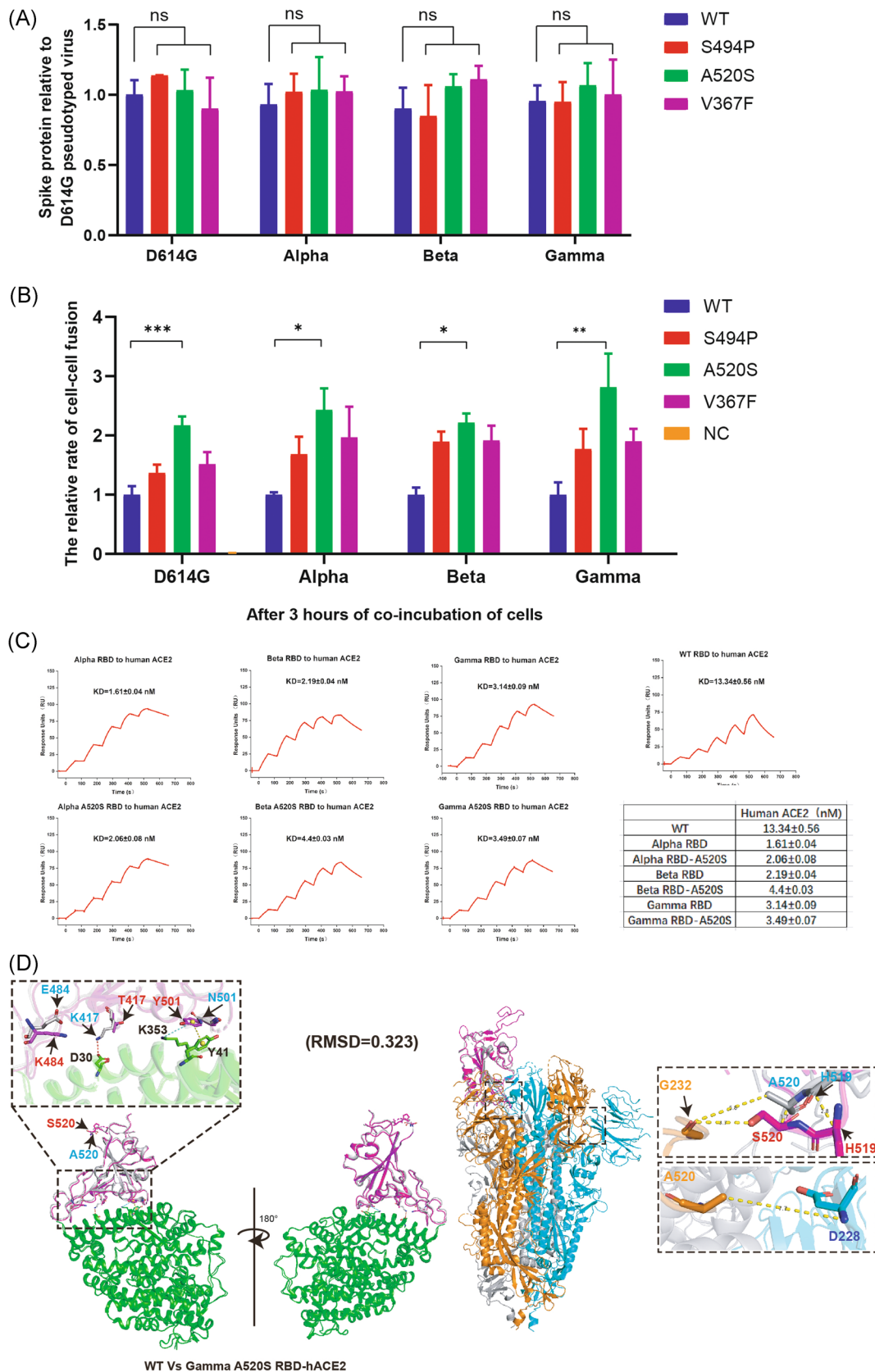
FIGURE 4 (See caption on next page)

mutations may be achieved through the pathway of cell–cell fusion enhancement. Among the three mutations, variants with A520S displayed a significant effect in increasing the cell–cell fusion. Thus, we focused on the A520S.

We first evaluated the effect of A520S on the binding affinity to the human receptor. As previously reported,[21,35] compared with the prototype RBD (WT), all the Alpha, Beta, and Gamma RBDs displayed increased binding strength to the human receptor (Figure 4C). When A520S was incorporated into the three VOCs, the affinities to hACE2 were maintained at a similar level to their respective parental ones.

We then solved the complex structure of Gamma-A520S RBD with hACE2 at a resolution of 3.3 Å. The structure of Gamma-A520S RBD-hACE2 was similar to the WT RBD-hACE2 structure with a root-mean-square deviation (RMSD) of 0.323 Å (for 737 Cα atoms, PDB: 6LZG). As indicated in Figure 4D, N501Y in the Gamma RBD induces little conformational change. However, due to the addition of the phenyl, Y501 seems to form a cation–π interaction with hACE2 K353 and a π–π stacking interaction with hACE2 Y41, conferring Gamma RBD higher binding affinity to the receptor than the parental N501, which has been observed by other groups.[35] The residue 520 does not involve the association with hACE2. Consistently, the three VOCs with A520 displayed similar binding affinities with hACE2 to those containing S520 (Figure 4C).

Notably, residue 520 at the trimeric S protein locates at the interface with the adjacent protomer NTD. When the complex structure of Gamma-A520S with hACE2 was superimposed with the Cryo-EM structure of S protein (PDB: 6VSB), the standing RBD S520 Cα is 1.7 Å closer to the adjacent NTD loop, compared with the A520 Cα. Accordingly, S520 was 2.1 Å closer to NTD G232, forming stronger interaction with G232 than A520 (Figure 4D). Although S520 in the lying RBD also brings RBD a little closer to the adjacent

NTD, from 6.8 to 6.1 Å, they still form relatively weak interaction. Thus, compared with A520, S520 in the standing RBD probably increases the interaction with NTD, thereby stabilizing the RBD at the standing conformation and favoring the binding to the receptor. Taken together, these may lead to enhanced infectivity of the possible Gamma+A520S virus.

3.4 | Analysis of neutralization changes in possible Alpha, Beta and Gamma variants with mAbs

Most mAbs against the RBD of spike protein showed high neutralization potency, and therefore mutations in the RBD are likely to cause a decrease in the neutralization potency of mAbs and even virus escape. Our study examined the neutralization activity of 12 mAbs from different isolated sources (including mAb CB6, which is already in clinical use) with possible Alpha, Beta, and Gamma variants. First, a fourfold decrease in neutralization protection was defined as mutation escape at this site. According to the neutralization results for 12 mAbs with possible Alpha variants (Figure 5A), the mutation sites that cause mAbs to lose neutralization protection can be classified into six categories. The neutralization results for the possible VOC single variants showed that the N501Y mutation escape the mAbs CB6 and 03-10D12-1C3, while the N501T substitution in the Alpha+N501T variant does not escape mAb 03-10D12-1C3 (Figure 5A); the mAbs BGB-DXP593, 05-9G11, MW07-LALA, AM128, AM180, and AbG3 were escaped by the E484K mutation, whereby DXP-593, 05-9G11, AM180, and AbG3 were also escaped by the L452R mutation; mAb DXP-604 was escaped by the K417N, but not the K417T mutation (Figure 5B); the mAb 09-4E5-1G2 was escaped by the N439K mutation; and the mAb 09-7B8 was escaped by the S477N, S477R, and T478K mutations. Encouragingly, we also identified a

FIGURE 4 Analysis of the effects of S494P, A520S, and V367F mutations on the spike protein and cell–cell fusion of different mutant strains of pseudotyped viruses. (A) After collecting the pseudotyped viruses, the viral RNA was first extracted and reverse transcribed into cDNA, then quantified by reverse transcription polymerase chain reaction. Finally, the WT, S494P, A520S, and V367F mutant pseudotyped viruses of the different mutant strains were diluted to the same particle number for an enzymw-linked immunosorbent assay assay to quantify the spike protein on the surface of the pseudotyped viruses. (B) The effect of pseudotyped viruses on cell–cell fusion was assessed by the detection of GFP fluorescence values. The 293T cells were transfected with GFP1-7 RLN plasmid and spike mutant plasmids of WT, S494P, A520S, and V367F of different mutant strain variants, and the 293T-ACE2 cells were transfected with GFP8-11 RLC plasmid. The cells were digested 24 h after transfection, and then mixed together and incubated for 3 h for GFP fluorescence detection. Using D614G as the reference strain, the relative GFP expression ratio, which represents the differential change in fusion between cells, was calculated. Data were replicated at least three times (mean ± SEM). *$p < 0.05$, **$p < 0.01$, ***$p < 0.005$, ****$p < 0.001$. (C) Binding affinity of SARS-CoV-2 RBDs to human ACE2, characterized by surface plasmon resonance. Mouse Fc (mFc)-fused hACE2 in the supernatant was captured in the CM5 chip via its interaction with the preimmobilized anti-mFc antibody. Serially diluted WT RBD, Alpha RBD, Alpha A520S RBD, Beta RBD, Beta A520S RBD, Gamma RBD, and Gamma A520S RBD protein flowed through the chip, and response unit was recorded. K_D values were calculated and the representative results from three experiments were shown. The data were presented as the mean ± SEM of three independent replicates ($n = 3$). (D) The overall structure of Gamma A520S RBD-hACE2. The complex structure of Gamma A520S RBD-hACE2 was superimposed on that of WT RBD-hACE2. Human ACE2, SARS-CoV-2 WT RBD, and Gamma A520S RBD were colored in green, gray, and magenta, respectively. The key contact residues were shown as stick structures and labeled appropriately. The cation–π interaction, π–π stacking interaction, and salt bridge were colored in cyan, yellow, and red, respectively. (E) Superimposition of Gamma A520S RBD in the complex on the Cryo-EM structure of SARS-CoV-2 spike glycoprotein (PDB: 6VSB) suggests that residue 520 in the RBD places in the interface with the adjacent NTD. The three protomers in the S protein were colored in gray, orange, and cyan, respectively. The Gamma A520S RBD was colored magenta. The key residues of RBD-A520, RBD-S520, NTD-D228, and NTD-G232 were marked with yellow dashed lines to show the interaction between them. GFP, green fluorescent protein; RBD, receptor-binding domain

FIGURE 5 Neutralizing monoclonal antibody sets for SARS-CoV-2 used to analyze antigenic changes in variants and possible mutant strains. Before cell processing, monoclonal antibodies were incubated with Alpha (A), Beta (B), and Gamma (C) possible mutant strains of pseudotyped viruses in a cell incubator at 37°C for 1 h before adding Huh7 cells for coculture. Luciferase activity was measured after 24 h to calculate the EC_{50} value for each antibody. The EC_{50} ratio between the variants or possible mutant strains and the reference strain D614G was calculated and analyzed to generate a heat map using Hem I.[36] Data are the result of at least three replicates. Red and blue boxes indicate enhanced or reduced neutralizing ability, respectively, as indicated by the specific degree of change, as shown on the graph scale
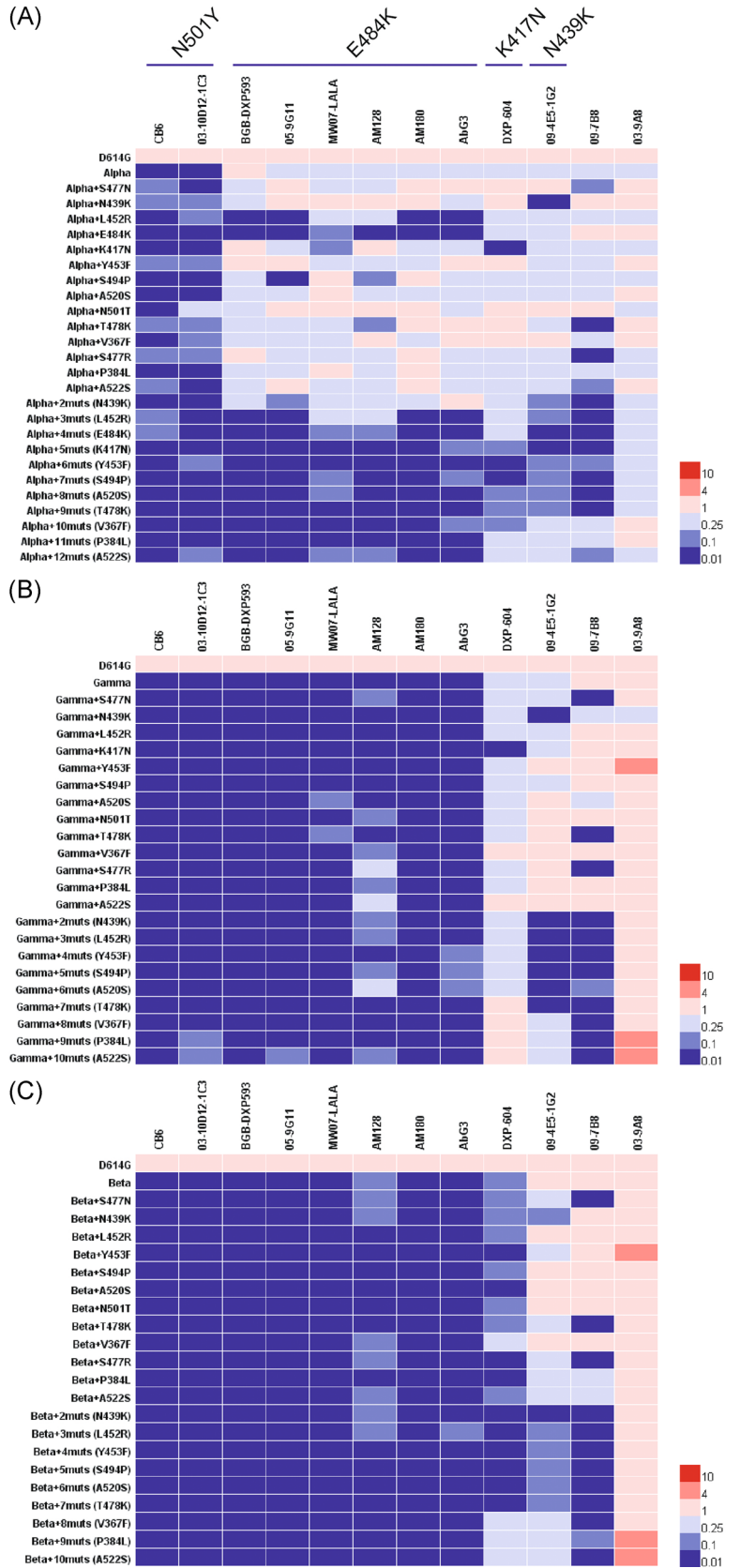
mAb—03-9A8—that showed good neutralizing effects (Figure 5) against all possible variants (including Beta and Gamma variants) and did not exhibit neutralizing escape against any pseudotyped virus used in this study. This suggested that mAb 03-9A8 is of clinical interest and deserves further investigation of the key binding sites to explain the mechanism by which the neutralization effect is not affected by these high-frequency RBD mutation sites. All possible multisite VOCs, when superimposed upon the single escape site described for the mAbs above, cause these mAbs to lose neutralization protection. For both Beta and Gamma possible pseudovirus variants, CB6, 03-10D12-1C3, DXP-593, 05-9G11, MW07-LALA, AM128, AM180, and AbG3 lost neutralization protection because they all have key N501, E484, and K417 site mutations in their RBDs (Figure 5B,C).

Interestingly, on the basis of the neutralization results, we found that some of the mutation sites enhanced the neutralization effect of mAbs when stacked together, with the last three sites of the top 15 high-frequency mutations—V367F, P384L, and A522S—being particularly effective at enhancing the neutralization of DXP-604 and 09-4E5-1G2 mAbs (Figure 5). To further investigate whether there is a synergistic effect between these three sites on pseudotyped virus neutralization, we performed one-, two- and three-site aggregated mutations on the D614G variant to verify their effects on neutralization. The results showed that in the neutralizing activity to the two mAbs, DXP-604 and 09-4E5-1G2, the D614G + V367F variant had a significantly higher neutralization effect compared with the D614G variant. D614G + P384L + A522S and D614G + V367F + P384L + A522S also had a significantly higher neutralization effect on the mAbs compared with the D614G variant pseudovirus, suggesting the possible synergistic effect of both P384L and A522S on neutralization protection (Figure S2A).

3.5 | Neutralization changes of the possible Alpha, Beta and Gamma variants against serum from convalescent patients

Next, we explored changes in the neutralizing potency of sera from convalescent patients against possible variants. For single-site mutations, the convalescent sera provided protection against the possible variants of the Alpha, Beta, and Gamma variants with no significant decrease (no more than 2.1-fold) compared with their corresponding VOC (Figure 6). Some possible variants, such as Alpha +V367F and Gamma+L452R, even showed a better neutralization ability to the convalescent sera (Figure 6A,C). The neutralizing activity of the convalescent sera to the Alpha and Gamma possible variants combined with multiple mutation sites was not significantly reduced, and still showed good protective efficacy. The largest decrease in neutralization protection among the possible Alpha and Gamma variants was seen for the Alpha strain combined with top 11 high-frequency RBD mutations, namely the Alpha+11muts (P384L) variant, which decreased only twofold relative to the Alpha variant (Figure 6A). Moreover, compared with the D614G variant, the above possible combined Alpha and Gamma variants also showed less than

a fourfold decrease in neutralization and did not display immune escape. Relative to the Beta variant, the decrease in the neutralizing activity of the convalescent sera to all Beta multisite combined possible variants was not significant, with a maximum doubling of the average titer (Figure 6B). However, it is noteworthy that the proportional decrease in the neutralization titer was more pronounced for the possible Beta multisite variants compared with the D614G strain combined with the second to tenth mutations, although the p values were not statistically significant (Figure 6B). The Beta variant showed the greatest decrease in neutralizing activity relative to Alpha and Gamma variants, but aggregation of 13 high-frequency RBD site substitutions on the variant also did not cause a significant decrease in neutralizing activity.

3.6 | Neutralization analysis of the possible Alpha, Beta, and Gamma variants with vaccine volunteer sera and guinea pig sera immunized with different immunogens

To further characterize the changes in neutralizing activity of three possible groups of VOCs against different human vaccine and antigen-immunized guinea pig sera, we detected two 2019-nCoV vaccine sera used in emergency trials or in clinical trials in China: the Ad5-Spike vaccine ($n = 5$) based on the adenoviral vector and the mRNA-Spike vaccine ($n = 4$), and also detected the sera from immunized guinea pig with four groups of immunogens: 2019-nCoV group ($n = 4$), D614G group ($n = 4$), D614G + E484K + N501Y group ($n = 4$), and D614G + K417N + E484K + N501Y group ($n = 4$). The results showed no significant changes in the neutralizing activity of either vaccine volunteer sera or guinea pig sera against the three groups of possible single point mutant strains of VOCs (Alpha, Beta, and Gamma), with mean neutralizing 50% of pseudotyped viral activity (NT_{50}) ratios relative to the corresponding VOCs of Ad5-Spike (2.16), mRNA-Spike (1.30), 2019-nCoV (1.45), D614G (1.37), D614G + E484K + N501Y (1.83), and D614G + K417N + E484K + N501Y (1.69) (Figure 7). For the possible aggregation of multiple mutated VOCs, the changes in their mean NT_{50} ratios relative to their respective parental VOCs were Ad5-Spike (1.15), mRNA-Spike (0.86), 2019-nCoV (1.28), D614G (1.04), D614G + E484K + N501Y (1.91), D614G + K417N + E484K + N501Y (1.42) (Figure 7). Among them, neutralizing activity of aggregated single-point and multipoint mutations on the possible VOCs suggested that the neutralization differences between immunogenic guinea pig sera with diverse mutations were insignificant, of which the immunoprotective effect of D614G + E484K + N501Y immunogen was slightly better than the other three groups. It is also noteworthy that the serum of vaccine volunteers (Ad5-Spike and mRNA-Spike) showed similar neutralization results to those of convalescent sera (Figure 6), with some possible multilocus aggregation variants of Beta showing near or slightly over a fourfold decrease in neutralization activity compared to the D614G strain due to a significant decrease in the Beta
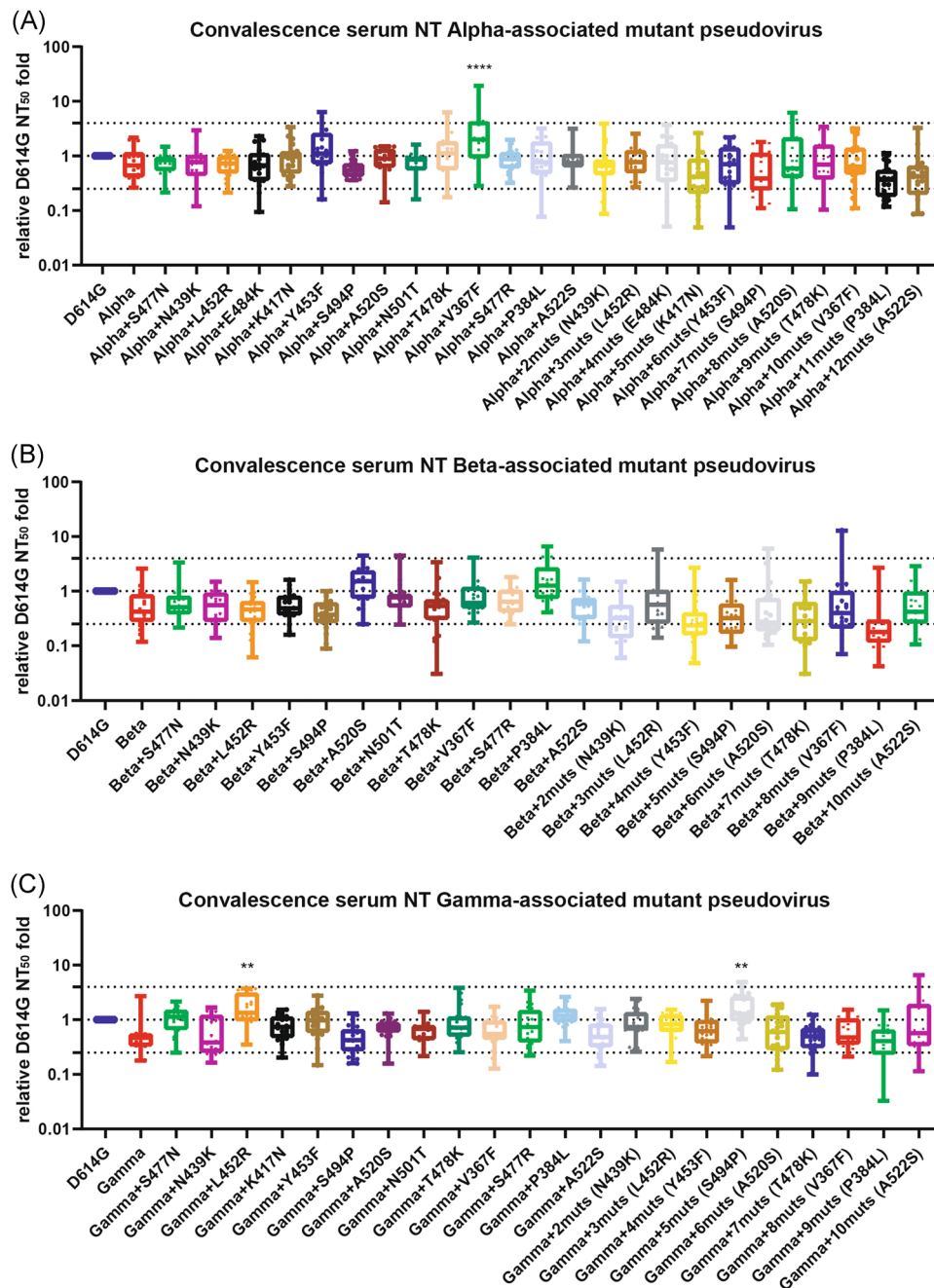
FIGURE 6 Convalescent serum from patients with SARS-CoV-2 for analysis of antigenic changes in natural variants and possible mutant strains. Before cell processing, convalescent sera (20 cases) were incubated with Alpha (A), Beta (B), and Gamma (C) possible mutant strains of pseudotyped viruses after threefold serial dilution at 37°C for 1 h and were then added to Huh7 cells for coculture. After 24 h, luciferase activity was measured to calculate the neutralizing 50% of pseudotyped viral activity (NT_{50}) value for each serum. The NT_{50} ratio between the variants or possible mutant strains and the reference strain D614G was calculated and analyzed to generate a heat map using Hem I. The dashed lines in the graph represent a fourfold increase or decrease in neutralization capacity compared with strain D614G, respectively. The horizontal line in the middle of the box represents the position of the median. The uppermost and lowermost horizontal dashed lines indicate the threshold lines for a four-fold change in the neutralization level relative to the reference strain D614G. Data are the result of at least three replicates. *$p < 0.05$, **$p < 0.01$, ***$p < 0.005$, ****$p < 0.001$

variant itself (Figure 7B). The above results suggested that the vast majority of the possible VOCs did not have more than a fourfold decrease in neutralizing activity relative to their corresponding VOCs, and the tendency was consistent with the performance of convalescent sera, which did not produce serious escapes, suggesting that the antigenic drift caused by RBD mutations in Spike proteins may not be as severe as feared, although it is certainly not possible to disregard the effects of RBD mutations.
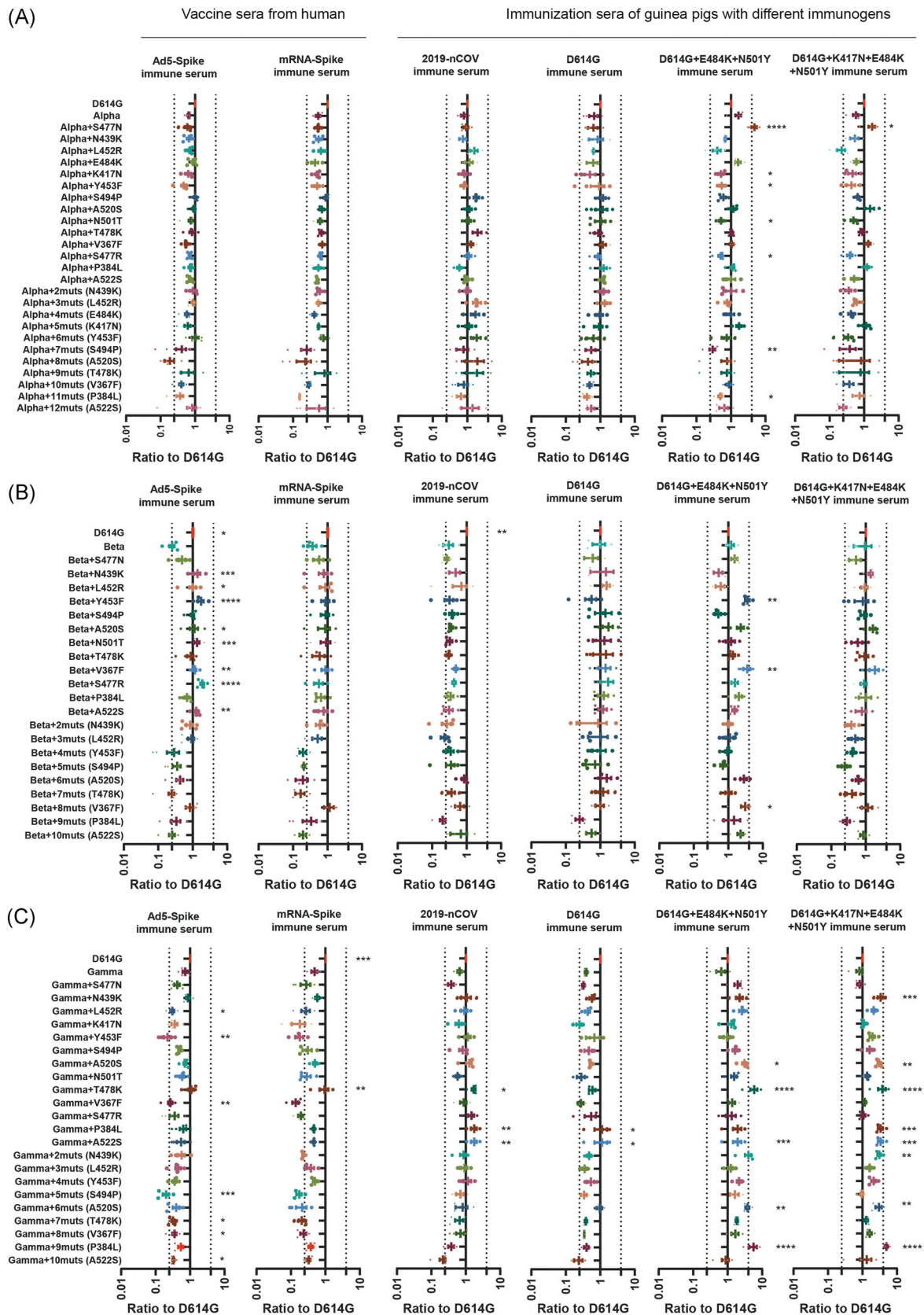
FIGURE 7 (See caption on next page)

4 | DISCUSSION

The long duration of the COVID-19 global pandemic, involving more than 230 million infections, has resulted in a vast pool of circulating viruses harboring complex and diversified mutations. Dozens of viral variants now exist, which include VOCs, VOIs, and variants under monitoring reports. The analysis of SARS-CoV-2 sequences uploaded from around the world has shown that certain mutants (e.g., D614G, L18S) predominate over time. For example, variant D614G has rapidly increased in prevalence, replacing the original variant in February 2020. It is possible that the rapid rise in this variant was the result of natural selection pressure, as this mutation significantly enhances the infectivity of the virus.[25] The subsequent Alpha, Beta, and Gamma epidemic variants were all based on the D614G variant, which suggests the predictive value of our studies combining mutations to individual VOCs. In this study, we attempted to understand in advance the changes in infectivity and antigenicity brought about by possible high-frequency RBD mutations in major VOCs. Such information could be potentially valuable in the prevention and control of future outbreaks.

Among the infectivity assays in this study, of particular interest was our finding that S494P, A520S, and V367F mutations enhance the infectivity of three VOCs in a variety of mammalian susceptible cells as well as ACE2-overexpressing 293T cells of different species. The S494P mutation has been reported to enhance the affinity of RBD to ACE2.[2] The V367F mutation was mainly found in the A.23.1 variant, which appears in Uganda and Vietnam, and has been suggested to enhance viral infectivity by increasing human ACE2 receptor-binding affinity.[37,38] Previous studies in our laboratory have shown that the V367F mutation in the original strain enhances susceptibility to mAbs and to sera from convalescent individuals.[7] In this study, both convalescent patient sera and different antigens immunized guinea pig sera showed significantly higher levels of neutralization with the D614G + V367F variant than the D614G strain (Figure S2B), suggesting that V367F does not pose a greater threat of increased protective efficacy in the vaccinated population. However, its elevated infectivity would exacerbate transmission in the unvaccinated population. Furthermore, the elevated infectivity and fusion capability following the combination of the A520S mutation with the Gamma variant was particularly notable. We found that this mutation exerted a slightly reduced binding affinity to the human receptor compared to their corresponding VOCs. Consistently, the complex structure of Gamma-A520S with hACE2 indicates that this residue does not involve receptor binding. This may be similar to the D614G mutation, which reduces the affinity with hACE2, S1 subunit is easier to dissociate and fall off after binding, increasing the chance of S2 subunit exposure and thus enhancing the fusion strength.[39,40] Meanwhile, in the complex structure, a little conformation change of the A520S-residing loop was observed. Notably, this loop places in the interface with the adjacent protomer NTD. This small conformational shift makes the S520 in the standing RBD closer to the adjacent NTD, thereby probably enhancing the interaction between the standing RBD with the NTD. Thus, the trimeric S with A520S probably possesses more standing RBD, and more readily interacts with the receptor to initiate the infections. Although this mutation also generally became more responsive to the neutralization of the convalescent sera in this study. Furthermore, a significant decrease in infectivity was found when multiple RBD mutations were aggregated with the possible Alpha, Beta, and Gamma variants compared with the D614G strain. The alteration of multiple RBD sites may negatively affect spike protein expression or folding maturation, suggesting that the combined multisite variants of live virus may also be at less risk of infection transmission.

Some variants (e.g., Alpha and Delta) of SARS-CoV-2 have been reported to show partial neutralization resistance to mAbs and vaccine sera.[41,42] However, our study found that convalescent patient sera, vaccine sera, and guinea pig sera immunized with different antigens showed a less than fourfold decrease in the neutralizing activity against single point mutations in possible Alpha, Beta, and Gamma variants, as well as most combination variants with up to 13 high-frequency mutation sites, compared with their corresponding VOCs. This indicated that the combination of up to 13 RBD high-frequency mutation sites in the Alpha, Beta, and Gamma variants does not lead to significant antigenic drift. Naturally, our vaccine serum samples and guinea pig sera should be further expanded to enrich our results. We know that vaccine efficacy depends on the specific recognition and activation of antigens by the human immune system.[43] That is, if mutations in the viral genome do not result in antigenic drift, then, in principle, the existing SARS-CoV-2 vaccines still do not lose their protective efficacy in the short term. This result is corroborated by the fact that current vaccines, such as mRNA-1273 and BNT162b2, maintained their effectiveness after two doses,

FIGURE 7 Analysis of antigenic changes in natural variants and possible mutant strains by SARS-CoV-2 vaccine sera and guinea pig sera immunized with different immunogens. The Ad5-Spike vaccine (five cases) based on the adenoviral vector, the mRNA-Spike vaccine (four cases), the 2019-nCoV-spike vaccine guinea pig sera (four cases), D614G-spike vaccine guinea pig sera (four cases), (D614G + E484K + N501Y)-spike vaccine guinea pig sera (four cases), and (D614G + K417N + E484K + N501Y)-spike vaccine guinea pig sera (four cases) were inactivated. Then, after threefold series of multiplicative dilutions, the sera were incubated with Alpha (A), Beta (B), and Gamma (C) possible mutant strains of pseudotyped viruses at 37°C for 1 h and then added to Huh7 cells for coculture. Luciferase activity was measured after 24 h to calculate the NT_{50} value for each serum. Using D614G as the reference strain, the NT_{50} ratio of the variants or possible mutant strains relative to the reference strain D614G was calculated and analyzed, and the neutralization mean values for each group were generated by GraphPad Prism 8.0. The dotted graph indicates the change in neutralization for each inoculator serum, with the dashed lines in the graph representing a fourfold increase or decrease in neutralization capacity compared with the D614G strain, respectively. p values were statistically calculated using the respective VOCs as control groups. Data are the result of at least three replicates (mean ± SEM). *$p < 0.05$, **$p < 0.01$, ***$p < 0.005$, ****$p < 0.001$

although a reduced neutralization effect was seen against variants such as Beta and Delta.[44–46] This may indicate a difference from influenza viruses, for which vaccine strains need to be changed frequently. Certain single amino acid changes on the hemagglutinin (HA) of the influenza virus (e.g., HA T135K) create a significant increase in antigenic distance, resulting in a dramatic decrease in vaccine sera neutralization potency.[47,48]

SARS-CoV-2 continues to evolve. New VOCs have emerged and spread rapidly. The presence of 15 RBD mutations aggregated in the Spike protein of the recently emerged variant Omicron, although the RBD mutations do not exactly overlap with that of our study, also predicts the possibility of the emergence of such variants with multi-RBD site mutations. As of November 2021, the first 10 mutation substitutions in RBD were infrequent. Only two mutations, E484Q and F490S, have increased the number of mutations into the first 10 positions compared to the start of this study in March. Thus, close monitoring for spike mutants and understanding potential complex variants in advance will be vital in the development of pandemic prevention and control strategies. In addition, mutations in the non-RBD region are also of interest, as one study reported that spike proteins are highly resistant to polyclonal neutralizing antibodies after more mutations in other regions such as NTD in addition to the RBD region.[49]

In conclusion, our study shows no severe decrease in neutralization protection against single mutant or multiple-RBD mutants of the 15 high-frequency in the three VOCs, suggesting that SARS-CoV-2 RBD mutations are not as prone to severe antigenic drift as influenza virus HA region mutations. This may alleviate concern that the vaccine must be updated as mutations in the RBD of spike protein continue to appear.[50] It is undeniable that as Spike proteins continue to accumulate mutations, serious antigenic drift may still occur, not excluding mutations caused by non-RBD regions, so it is suggested that vaccine research can continuously optimize the immunoprotective efficacy of vaccines (e.g., dose and frequency of booster immunization injections) while also focusing on the neutralizing efficacy of heterologous immunizations (different variants or different regions such as NTD- and RBD-specific antigens) to cope with the emerging new viral variants.

AUTHOR CONTRIBUTIONS

Youchun Wang, Qihui Wang, and Weijin Huang conceived, designed, and supervised the experiments. Tao Li and Youchun Wang wrote the manuscript. Tao Li, Zhimin Cui, Yunfei Jia, Ziteng Liang, Jianhui Nie, Li Zhang, Qianqian Li, Jiajing Wu, Shuo Liu, Xueli Li, Yimeng An, Pu Han, and Mengyi Zhang performed the experiments. Yuhua Li and Xiaowang Qu provided sera from vaccinated individuals and convalescing patients. All the authors have read and approved the final manuscript.

DATA AVAILABILITY STATEMENT

The data that support the findings of this study are available from the corresponding author upon reasonable request.

REFERENCES

1. Mateus J, Grifoni A, Tarke A, et al. Structure of the SARS-CoV-2 spike receptor-binding domain bound to the ACE2 receptor. *Nature*. 2020;581(7807):215-220.
2. Lopez E, Haycroft ER, Adair A, et al. Simultaneous evaluation of antibodies that inhibit SARS-CoV-2 variants via multiplex assay. *JCI Insight*. 2021;6(16):e150012.
3. Barnes CO, Jette CA, Abernathy ME, et al. SARS-CoV-2 neutralizing antibody structures inform therapeutic strategies. *Nature*. 2020;588(7839):682-687.
4. Baum A, Fulton BO, Wloga E, et al. Antibody cocktail to SARS-CoV-2 spike protein prevents rapid mutational escape seen with individual antibodies. *Science*. 2020;369(6506):1014-1018.
5. Greaney AJ, Starr TN, Gilchuk P, et al. Complete mapping of mutations to the SARS-CoV-2 spike receptor-binding domain that escape antibody recognition. *Cell Host Microbe*. 2021;29(1):44-57.
6. Greaney AJ, Starr TN, Gilchuk P, et al. Complete mapping of mutations to the SARS-CoV-2 spike receptor-binding domain that escape antibody recognition. *Cell Host Microbe*. 2021;29(1):44-57.e49.
7. Li Q, Wu J, Nie J, et al. The impact of mutations in SARS-CoV-2 spike on viral infectivity and antigenicity. *Cell*. 2020;182(5):1284-1294.e1289.
8. Yi C, Sun X, Ye J, et al. Key residues of the receptor binding motif in the spike protein of SARS-CoV-2 that interact with ACE2 and neutralizing antibodies. *Cell Mol Immunol*. 2020;17(6):621-630.
9. Shang J, Ye G, Shi K, et al. Structural basis of receptor recognition by SARS-CoV-2. *Nature*. 2020;581(7807):221-224.
10. Leung K, Shum MHH, Leung GM, Lam TTY, Wu JT. Early transmissibility assessment of the N501Y mutant strains of SARS-CoV-2 in the United Kingdom, October to November 2020. *Euro Surveill*. 2021;26(1).
11. Volz E, Mishra S, Chand M, et al. Assessing transmissibility of SARS-CoV-2 lineage B.1.1.7 in England. *Nature*. 2021;593(7858):266-269.
12. Callaway E, Mallapaty S. Novavax offers first evidence that COVID vaccines protect people against variants. *Nature*. 2021;590(7844):17-17.
13. Morales AC, Rice AM, Ho AT, et al. Causes and consequences of purifying selection on SARS-CoV-2. *Genome Biol Evol*. 2021;13:10.
14. Nie J, Li Q, Wu J, et al. Establishment and validation of a pseudovirus neutralization assay for SARS-CoV-2. *Emerg Microbes Infect*. 2020;9(1):680-686.
15. Nie J, Li Q, Wu J, et al. Quantification of SARS-CoV-2 neutralizing antibody by a pseudotyped virus-based assay. *Nat Protoc*. 2020;15(11):3699-3715.

16. Li Q, Nie J, Wu J, et al. SARS-CoV-2 501Y.V2 variants lack higher infectivity but do have immune escape. *Cell*. 2021;184(9): 2362-2371.e2369.

17. Kondo N, Miyauchi K, Meng F, Iwamoto A, Matsuda Z. Conformational changes of the HIV-1 envelope protein during membrane fusion are inhibited by the replacement of its membrane-spanning domain. *J Biol Chem*. 2010;285(19):14681-14688.

18. Thakur N, Conceicao C, Isaacs A, et al. Micro-fusion inhibition tests: quantifying antibody neutralization of virus-mediated cell–cell fusion. *J Gen Virol*. 2021;102(1).

19. Wu L, Chen Q, Liu K, et al. Broad host range of SARS-CoV-2 and the molecular basis for SARS-CoV-2 binding to cat ACE2. *Cell Discov*. 2020;6(1):68.

20. Wang Q, Zhang Y, Wu L, et al. Structural and functional basis of SARS-CoV-2 entry by using human ACE2. *Cell*. 2020;181(4): 894-904.e899.

21. Han P, Su C, Zhang Y, et al. Molecular insights into receptor binding of recent emerging SARS-CoV-2 variants. *Nat Commun*. 2021;12(1): 6103.

22. Otwinowski Z, Minor W. Processing of X-ray diffraction data collected in oscillation mode. *Methods Enzymol*. 1997;276:307-326.

23. Adams PD, Afonine PV, Bunkóczi G, et al. PHENIX: a comprehensive Python-based system for macromolecular structure solution. *Acta Crystallograph D Biol Crystallogr*. 2010;66(2):213-221.

24. Emsley P, Cowtan K. Coot: model-building tools for molecular graphics. *Acta Crystallogr D Biol Crystallogr*. 2004;60(Pt 12 Pt 1): 2126-2132.

25. Yang J, Wang W, Chen Z, et al. A vaccine targeting the RBD of the S protein of SARS-CoV-2 induces protective immunity. *Nature*. 2020; 586(7830):572-577.

26. Koyama T, Platt D, Parida L. Variant analysis of SARS-CoV-2 genomes. *Bull World Health Organ*. 2020;98(7):495-504.

27. Callaway E. The coronavirus is mutating—does it matter? *Nature*. 2020;585(7824):174-177.

28. Hoffmann M, Kleine-Weber H, Schroeder S, et al. SARS-CoV-2 cell entry depends on ACE2 and TMPRSS2 and is blocked by a clinically proven protease inhibitor. *Cell*. 2020;181(2):271-280.e278.

29. Abbasi AZ, Kiyani DA, Hamid SM, Saalim M, Fahim A, Jalal N. Spiking dependence of SARS-CoV-2 pathogenicity on TMPRSS2. *J Med Virol*. 2021;93(7):4205-4218.

30. Torre-Fuentes L, Matías-Guiu J, Hernández-Lorenzo L, et al. ACE2, TMPRSS2, and Furin variants and SARS-CoV-2 infection in Madrid, Spain. *J Med Virol*. 2021;93(2):863-869.

31. Jackson CB, Farzan M, Chen B, Choe H. Mechanisms of SARS-CoV-2 entry into cells. *Nat Rev Mol Cell Biol*. 2021;23(1):3-20.

32. Oude Munnink BB, Sikkema RS, Nieuwenhuijse DF, et al. Transmission of SARS-CoV-2 on mink farms between humans and mink and back to humans. *Science*. 2021;371(6525):172-177.

33. Hu B, Guo H, Zhou P, Shi Z-L. Characteristics of SARS-CoV-2 and COVID-19. *Nat Rev Microbiol*. 2020;19(3):141-154.

34. Boni MF, Lemey P, Jiang X, et al. Evolutionary origins of the SARS-CoV-2 sarbecovirus lineage responsible for the COVID-19 pandemic. *Nat Microbiol*. 2020;5(11):1408-1417.

35. Zhu X, Mannar D, Srivastava SS, et al. Cryo-electron microscopy structures of the N501Y SARS-CoV-2 spike protein in complex with ACE2 and 2 potent neutralizing antibodies. *PLoS Biol*. 2021;19(4): e3001237.

36. Zhang Z, Deng W, Wang Y, Liu Z, Cheng H, Xue Y. eml: a toolkit for illustrating heatmaps. *PLoS One*. 2014;9(11):e111988.

37. Ge J, Wang R, Ju B, et al. Antibody neutralization of SARS-CoV-2 through ACE2 receptor mimicry. *Nat Commun*. 2021;12(1):250.

38. Chen J, Wang R, Wang M, Wei G-W. Mutations strengthened SARS-CoV-2 infectivity. *J Mol Biol*. 2020;432(19):5212-5226.

39. Jiang X, Zhang Z, Wang C, et al. Bimodular effects of D614G mutation on the spike glycoprotein of SARS-CoV-2 enhance protein processing, membrane fusion, and viral infectivity. *Signal Transduct Target Ther*. 2020;5(1):268.

40. Yurkovetskiy L, Wang X, Pascal KE, et al. Structural and functional analysis of the D614G SARS-CoV-2 spike protein variant. *Cell*. 2020; 183(3):739-751.e738.

41. Planas D, Veyer D, Baidaliuk A, et al. Reduced sensitivity of SARS-CoV-2 variant Delta to antibody neutralization. *Nature*. 2021; 596(7871):276-280.

42. Liu C, Ginn HM, Dejnirattisai W, et al. Reduced neutralization of SARS-CoV-2 B.1.617 by vaccine and convalescent serum. *Cell*. 2021;184(16):4220-4236.e4213.

43. Mateus J, Grifoni A, Tarke A, et al. Selective and cross-reactive SARS-CoV-2 T cell epitopes in unexposed humans. *Science*. 2020; 370(6512):89-94.

44. Noori M, Nejadghaderi SA, Arshi S, et al. Potency of BNT162b2 and mRNA-1273 vaccine-induced neutralizing antibodies against severe acute respiratory syndrome-CoV-2 variants of concern: a systematic review of in vitro studies. *Rev Med Virol*. 2021:e2277.

45. Pegu A, O'connell SE, Schmidt SD, et al. Durability of mRNA-1273 vaccine–induced antibodies against SARS-CoV-2 variants. *Science*. 2021;373(6561):1372-1377.

46. Lopez Bernal J, Andrews N, Gower C, et al. Effectiveness of Covid-19 vaccines against the B.1.617.2 (Delta) variant. *N Engl J Med*. 2021;385(7):585-594.

47. Jorquera PA, Mishin VP, Chesnokov A, et al. Insights into the antigenic advancement of influenza A(H3N2) viruses, 2011–2018. *Sci Rep*. 2019;9(1):2676.

48. Koel BF, Burke DF, Bestebroer TM, et al. Substitutions near the receptor binding site determine major antigenic change during influenza virus evolution. *Science*. 2013;342(6161):976-979.

49. Schmidt F, Weisblum Y, Rutkowska M, et al. High genetic barrier to SARS-CoV-2 polyclonal neutralizing antibody escape. *Nature*. 2021; 600(7889):512-516.

50. Subbarao K. The success of SARS-CoV-2 vaccines and challenges ahead. *Cell Host Microbe*. 2021;29(7):1111-1123.

SUPPORTING INFORMATION

Additional supporting information may be found in the online version of the article at the publisher's website.